NASA/TM—2003-212383 AIAA–2003–3254

Computation of Large-Scale Structure Jet Noise Sources With Weak Nonlinear Effects Using Linear Euler

Milo D. Dahl
Glenn Research Center, Cleveland, Ohio

Ray Hixon
University of Toledo, Toledo, Ohio

Reda R. Mankbadi
Embry-Riddle Aeronautical University, Daytona Beach, Florida

July 2003

The NASA STI Program Office . . . in Profile

Since its founding, NASA has been dedicated to the advancement of aeronautics and space science. The NASA Scientific and Technical Information (STI) Program Office plays a key part in helping NASA maintain this important role.

The NASA STI Program Office is operated by Langley Research Center, the Lead Center for NASA's scientific and technical information. The NASA STI Program Office provides access to the NASA STI Database, the largest collection of aeronautical and space science STI in the world. The Program Office is also NASA's institutional mechanism for disseminating the results of its research and development activities. These results are published by NASA in the NASA STI Report Series, which includes the following report types:

- TECHNICAL PUBLICATION. Reports of completed research or a major significant phase of research that present the results of NASA programs and include extensive data or theoretical analysis. Includes compilations of significant scientific and technical data and information deemed to be of continuing reference value. NASA's counterpart of peer-reviewed formal professional papers but has less stringent limitations on manuscript length and extent of graphic presentations.

- TECHNICAL MEMORANDUM. Scientific and technical findings that are preliminary or of specialized interest, e.g., quick release reports, working papers, and bibliographies that contain minimal annotation. Does not contain extensive analysis.

- CONTRACTOR REPORT. Scientific and technical findings by NASA-sponsored contractors and grantees.

- CONFERENCE PUBLICATION. Collected papers from scientific and technical conferences, symposia, seminars, or other meetings sponsored or cosponsored by NASA.

- SPECIAL PUBLICATION. Scientific, technical, or historical information from NASA programs, projects, and missions, often concerned with subjects having substantial public interest.

- TECHNICAL TRANSLATION. English-language translations of foreign scientific and technical material pertinent to NASA's mission.

Specialized services that complement the STI Program Office's diverse offerings include creating custom thesauri, building customized databases, organizing and publishing research results . . . even providing videos.

For more information about the NASA STI Program Office, see the following:

- Access the NASA STI Program Home Page at ***http://www.sti.nasa.gov***

- E-mail your question via the Internet to help@sti.nasa.gov

- Fax your question to the NASA Access Help Desk at 301–621–0134

- Telephone the NASA Access Help Desk at 301–621–0390

- Write to:
  NASA Access Help Desk
  NASA Center for AeroSpace Information
  7121 Standard Drive
  Hanover, MD 21076

NASA/TM—2003-212383 AIAA–2003–3254

Computation of Large-Scale Structure Jet Noise Sources With Weak Nonlinear Effects Using Linear Euler

Milo D. Dahl
Glenn Research Center, Cleveland, Ohio

Ray Hixon
University of Toledo, Toledo, Ohio

Reda R. Mankbadi
Embry-Riddle Aeronautical University, Daytona Beach, Florida

Prepared for the
Nineth Aeroacoustics Conference and Exhibit
cosponsored by the American Institute of Aeronautics and Astronautics
and the Confederation of European Aerospace Societies
Hilton Head, South Carolina, May 12–14, 2003

National Aeronautics and
Space Administration

Glenn Research Center

July 2003

Available from

NASA Center for Aerospace Information
7121 Standard Drive
Hanover, MD 21076

National Technical Information Service
5285 Port Royal Road
Springfield, VA 22100

Available electronically at http://gltrs.grc.nasa.gov

COMPUTATION OF LARGE-SCALE STRUCTURE JET NOISE SOURCES WITH WEAK NONLINEAR EFFECTS USING LINEAR EULER

Milo D. Dahl[*]
National Aeronautics and Space Administration
Glenn Research Center
Cleveland, OH 44135

Ray Hixon[†]
University of Toledo
Toledo, OH 43606

Reda R. Mankbadi[‡]
Embry-Riddle Aeronautical University
Daytona Beach, FL 32114

ABSTRACT

An approximate technique is presented for the prediction of the large-scale turbulent structure sound source in a supersonic jet. A linearized Euler equations code is used to solve for the flow disturbances within and near a jet with a given mean flow. Assuming a normal mode composition for the wave-like disturbances, the linear radial profiles are used in an integration of the Navier-Stokes equations. This results in a set of ordinary differential equations representing the weakly nonlinear self-interactions of the modes along with their interaction with the mean flow. Solutions are then used to correct the amplitude of the disturbances that represent the source of large-scale turbulent structure sound in the jet.

INTRODUCTION

While considerable progress has been made over the last decade toward the prediction of jet noise, an efficient tool for the prediction of jet noise in practical geometries is still lacking. The problem can be split into the prediction of the source field and the prediction of the acoustic field associated with it. As for the latter, there are now a number of schemes that can successfully predict the acoustic field associated with a well-prescribed sound source. In the acoustic analogy approach, time-average correlations can be used to construct the acoustic source.[1] This source is used in a volume integration to obtain the acoustic field. An implementation of this approach is described by Khavaran[2] where the statistical properties of the noise sources are described by two-point, space-time correlation models derived from RANS solutions for the flow field using k-ϵ turbulence models. An alternative approach was recently developed by Tam & Auriault[3] where models for the two-point correlations are given in a fixed reference frame, rather than the moving reference frame commonly used in previous approaches. In both of these approaches, it is the fine-scale turbulence that is modeled as the source of noise.

Strong evidence suggests that jet noise, particularly in the supersonic regime, has contributions from large-scale turbulent or wave-like structures in the initial region in the jet and can be the dominant noise source. These structures cannot be captured by classical turbulence modeling. Direct Numerical Simulations (DNS) and Large Eddy Simulations (LES) can successfully capture these structures, but they are computationally intensive.

Large-Eddy Simulations (LES) is the most promising approach for prediction of the noise source. The resolution in LES involving the acoustic field is usually selected such that all the acoustically relevant scales are resolved. In principal, LES can be extended to resolve all the scales as in DNS by making the resolution equivalent to that of DNS. At the other end, the computations can be made less CPU intensive by selecting a coarse mesh, and resolving only the very-large scales (VLES). Although VLES may be less CPU intensive compared to LES, still there is an obvious need to develop an approximate, but fast approach for prediction of jet noise.

The work presented herein focuses on predicting the noise source associated with the large-scale, low frequency noise. This work, along with a parallel work for prediction of the small-scale noise, should provide a practical tool for prediction of jet noise associated with both the small and large scales. The basic idea herein is to first neglect nonlinearity and use a Linearized Euler Equations (LEE) code to predict the time-dependent source in a given mean flow. Nonlinear effects are then accounted for via a nonlinear integral technique similar to that of Dahl & Mankbadi.[4]

The starting point of this analysis is that we consider a turbulent round jet at a sufficiently high speed so that the compressibility is significant. The development of this jet in the unexcited case is assumed to be given by some other means (e.g. analytically or via Reynolds averaged numerical simulations). This jet is then excited by a single-

[*]Research Scientist, Member AIAA
[†]Assistant Professor, Member AIAA
[‡]Dean, College of Engineering, Associate Fellow AIAA

frequency instability wave. The nonlinear development of this wave will be presented herein based on the integral energy approach. Along with the wave development, the mean flow-spreading rate is also modified. Since the focus here is the supersonic jet, we must consider the helical modes as they are more amplified than the axisymmetric ones. Once the computations are completed, a description of all the variables of the large-structure disturbance field in and near the jet is given for a particular mode number and frequency. It can be used as the acoustic source to compute the noise radiation field outside of the jet. This is described in a separate paper.[5]

In the next section, we describe the LEE method used to compute the large-scale turbulent disturbances. The advantage of this approach is that it allows the base mean flow to be non-parallel. This has the consequence that the numerical singularities, present in the previous locally-parallel stability analysis,[4] are eliminated. The development of the integral energy equations is described in the following two sections. Finally, results are shown for the nonlinear calculations showing the effects of dissipation, initial large-scale structure amplitude, and jet Mach number on the spatial evolution of the amplitude and phase of the structure.

LINEARIZED EULER EQUATIONS

Consider a high-Reynolds number turbulent jet issuing from a nozzle of diameter D in a still air. The jet is shock-free, but the Mach number is high enough for compressibility effects to be significant. The density and the component velocities are normalized by the jet exit density and axial velocity at the centerline, ρ_j and U_j, respectively. The pressure is normalized by $\rho_j U_j^2$, time by D/U_j, and spatial coordinates by D. Each flow parameter is split into a time-averaged part $\overline{U}_i(x,r,\phi)$ and a disturbance part, $u_i'(x,r,\phi,t)$. Thus, the velocity can be written :

$$u_i = \overline{U}_i(x,r,\phi) + u_i'(x,r,\phi,t) \tag{1}$$

where $i = 1,2,3$. In the cylindrical coordinates, 1 refers to the axial direction x with axial velocity u, 2 refers to the radial direction r with radial velocity v, and 3 refers to the azimuthal direction ϕ with azimuthal velocity w. An over bar, $\overline{(\quad)}$, denotes a time-averaged quantity. The pressure and the density are similarly split:

$$p = \overline{P}(x,r,\phi) + p'(x,r,\phi,t) \tag{2}$$

$$\rho = \overline{\rho}(x,r,\phi) + \rho'(x,r,\phi,t) \tag{3}$$

For the product of the density with the velocities, we get

$$\rho u_i = (\overline{\rho} + \rho')(\overline{U}_i + u_i') = \overline{\rho}\,\overline{U}_i + \overline{\rho}\,u_i' + \rho'\,\overline{U}_i + \rho' u_i'$$

Time-averaging yields

$$\overline{\rho u_i} = \overline{\rho}\,\overline{U}_i + \overline{\rho' u_i'} \tag{4}$$

and we define

$$\widetilde{\rho u_i} \equiv \rho u_i - \overline{\rho u_i} = \overline{\rho}\,u_i' + \rho'\,\overline{U}_i + \rho' u_i' - \overline{\rho' u_i'}. \tag{5}$$

Thus, we get

$$\rho u_i = \overline{\rho u_i} + \widetilde{\rho u_i}. \tag{6}$$

Starting from the full Navier-Stokes equations in conservative form, we neglect viscosity, linearize about a given mean flow and separate the disturbance variables into azimuthal modes by assuming the presence of an $\exp(in\phi)$ factor in each variable. The resulting Linearized Euler equations may be written in cylindrical coordinates as follows:

$$(r\boldsymbol{Q})_t + (r\boldsymbol{F})_x + (r\boldsymbol{G})_r + in\boldsymbol{H} = \boldsymbol{S} \tag{7}$$

where n is the azimuthal mode number and the vector quantities are:

$$\boldsymbol{Q} = \left[\rho' \;\; \widetilde{\rho v} \;\; \widetilde{\rho w} \;\; \widetilde{\rho u} \;\; e'\right]^T$$

$$\boldsymbol{F} = \begin{bmatrix} \widetilde{\rho u} \\ -\rho'\overline{V}\,\overline{U} + \widetilde{\rho v}\,\overline{U} + \widetilde{\rho u}\,\overline{V} \\ -\rho'\overline{W}\,\overline{U} + \widetilde{\rho w}\,\overline{U} + \widetilde{\rho u}\,\overline{W} \\ -\rho'\overline{U}\,\overline{U} + 2\widetilde{\rho u}\,\overline{U} + p' \\ \overline{U}(p'+e') + (\widetilde{\rho u} - \rho'\overline{U})\left(\dfrac{\overline{P}+\overline{E}}{\overline{\rho}}\right) \end{bmatrix}$$

$$\boldsymbol{G} = \begin{bmatrix} \widetilde{\rho v} \\ -\rho'\overline{V}\,\overline{V} + 2\widetilde{\rho v}\,\overline{V} + p' \\ -\rho'\overline{V}\,\overline{W} + \widetilde{\rho w}\,\overline{V} + \widetilde{\rho v}\,\overline{W} \\ -\rho'\overline{V}\,\overline{U} + \widetilde{\rho u}\,\overline{V} + \widetilde{\rho v}\,\overline{U} \\ \overline{V}(p'+e') + (\widetilde{\rho v} - \rho'\overline{V})\left(\dfrac{\overline{P}+\overline{E}}{\overline{\rho}}\right) \end{bmatrix}$$

$$\boldsymbol{H} = \begin{bmatrix} \widetilde{\rho w} \\ -\rho'\overline{V}\,\overline{W} + \widetilde{\rho v}\,\overline{W} + \widetilde{\rho w}\,\overline{V} \\ -\rho'\overline{W}\,\overline{W} + 2\widetilde{\rho w}\,\overline{W} + p' \\ -\rho'\overline{U}\,\overline{W} + \widetilde{\rho u}\,\overline{W} + \widetilde{\rho w}\,\overline{U} \\ \overline{W}(p'+e') + (\widetilde{\rho w} - \rho'\overline{W})\left(\dfrac{\overline{P}+\overline{E}}{\overline{\rho}}\right) \end{bmatrix}$$

$$\boldsymbol{S} = \begin{bmatrix} 0 \\ -\rho'\overline{W}\,\overline{W} + 2\widetilde{\rho w}\,\overline{W} + p' \\ \rho'\overline{V}\,\overline{W} - \widetilde{\rho w}\,\overline{V} - \widetilde{\rho v}\,\overline{W} \\ 0 \\ 0 \end{bmatrix}$$

where the mean and the disturbance pressures are given by

$$\overline{P} = (\gamma-1)\left[\overline{E} - \frac{1}{2}\overline{\rho}(\overline{U}^2 + \overline{V}^2 + \overline{W}^2)\right]$$

$$p' = (\gamma-1)\Big[e' - (\widetilde{\rho u}\,\overline{U} + \widetilde{\rho v}\,\overline{V} + \widetilde{\rho w}\,\overline{W}) + \frac{1}{2}\rho'(\overline{U}^2 + \overline{V}^2 + \overline{W}^2)\Big]$$

$\overline{E}$ is the mean total energy and e' is the energy disturbance variable. In developing the Linearized Euler equations, only the linear terms of equation (5) for $\widetilde{\rho u_i}$ are retained.

In this formulation, each additional mode calculated adds another set of equations to be solved. The advantages to this formulation are lowered storage and computation, improved centerline behavior, and improved boundary condition specification.

Numerical algorithm

The code uses an explicit time-marching method coupled with central differences in space. To eliminate spurious high-wavenumber oscillations, artificial dissipation is employed. For computational efficiency and maximum compiler optimization, the code is written in FORTRAN 77.

The time marching method is a low-storage, fourth-order extension of an optimized LDDRK 5-6 method.[6,7] For accurate spatial differencing, the 7-point DRP method of Tam & Webb is used.[8] For artificial viscosity, an explicit 10th order dissipation is used.[9]

Computational grid

The grid used for the cases computed for this paper had 171 (radial) x 251 (axial) grid points. In the radial direction, the grid started with the minimum spacing of $\Delta r/D = 0.02$ at the centerline and smoothly stretching to 0.15 at $r/D = 16$. In the axial direction, the minimum spacing was $\Delta x/D = 0.02$ at the $x = 0$ boundary and smoothly stretching to 0.15 at the $x/D = 35$ boundary. The maximum spacing corresponds to 10 points per wavelength, which is well within the accuracy range of this code. All cases used the same computational grid. A Courant number of 1.4 was used for these computations.

Boundary conditions

Special attention is given to the boundary treatment in order to avoid non-physical oscillations, which can render the computed unsteady solution unacceptable. Several boundary treatments were considered. The boundary treatments follow that of Mankbadi et al.[10] At the inflow, Thompson, non-reflecting boundary treatment is implemented. The conventional acoustic radiation condition is applied at the radiation boundaries, which are defined at inflow, $x = 0$, where $r/D > 2$, and at the outflow, $x = x_{max}$, for all radial points where the Mach number is less than 0.01. For $r = r_{max}$, the radiation condition is applied to all x-points. At the outflow, where the Mach number is greater than 0.01, the Tam & Webb[8] asymptotic boundary treatment is applied. In this code, the centerline boundary is represented with a point at the centerline, and a ghost point reflected across the centerline in the radial direction. Without azimuthal mode decomposition, the centerline treatment for a three- dimensional problem is not straightforward, and was addressed by Shih et al.[11] However, using the azimuthal mode decomposition method, the centerline boundary condition becomes straightforward:

$$r \left[G_1 \; G_2 \; G_3 \; G_4 \; G_5\right]^T_{r=0} = 0$$

and

$$r \left[G_1 \; G_2 \; G_3 \; G_4 \; G_5\right]^T_{r=-\Delta r} = r \left[G_1 \; -G_2 \; -G_3 \; G_4 \; G_5\right]^T_{r=\Delta r} e^{in\pi}$$

where G_1 to G_5 represent the five terms in the $\boldsymbol{G}$ vector in equation (7).

Inflow disturbance

At the inflow boundary, $x/D = 0$, a disturbance based on the linear stability eigenmodes for the inflow jet profile is introduced:

$$\boldsymbol{Q} = L_{\boldsymbol{Q}}(r) e^{i\omega t}$$

where $L_{\boldsymbol{Q}}(r)$ represents the radial eigenvector of the linear stability wave for the set of disturbance variables. To introduce the input disturbance into the flow field, the time derivatives of the disturbance are added to the computed flow variables at each time step:

$$\boldsymbol{Q}_{t,final} = \boldsymbol{Q}_{t,BC} + i\omega L_{\boldsymbol{Q}}(r) e^{i\omega t}$$

This boundary condition inputs the locally-parallel eigenfunction solution that is not exactly equivalent to the Euler solution. This difference results in a transient wave near the inflow boundary causing inaccuracies in the numerical results.

WEAKLY NONLINEAR EFFECTS

The source predicted by LEE neglects nonlinear effects. However, nonlinear effects seem to be important and need to be taken into account. Dahl & Mankbadi[4] developed a nonlinear technique for the prediction of the noise source associated with instability waves in a compressible jet. In their work, the partial differential equations were integrated across the transverse direction assuming that the disturbance profiles were given by the eigenfunctions of a locally-parallel, viscous, linear stability calculation. Certain mathematical singularities that occurred within the stability equations of this approach limited its usefulness. In addition, the integral energy equations of the previous paper contain some inconsistencies that are resolved in the presentation below. In the present work, the disturbance variable profiles will be taken from the linear Euler solution.

Shape assumptions

In the integral energy method, the system of equations is integrated in the radial direction using shape assumptions for the disturbance variables. The disturbances, considered to be the large-scale turbulent structures, are assumed to have the form of a traveling wave. Following the work of

Lee & Liu,[12] the waves are assumed separable into an unknown amplitude function and a radial shape function

$$\begin{pmatrix} u_i'(x,r,\phi,t) \\ p'(x,r,\phi,t) \\ \rho'(x,r,\phi,t) \end{pmatrix} = A(x)e^{i\psi(x)} \begin{pmatrix} \hat{u}_i(r) \\ \hat{p}(r) \\ \hat{\rho}(r) \end{pmatrix} \exp(\Psi) \quad (8)$$

$$\Psi = -i\omega t + in\phi$$

with an axial phase function $\psi(x)$ that also needs to be determined. In equation (8), $(\hat{})$ denotes the radial shape function of the transverse coordinate r at a given location along the jet. $\hat{u}_i(r)$, $\hat{p}(r)$, and $\hat{\rho}(r)$ are radial shapes computed by the LEE code at a given axial location and at a given n and ω. Here, n is the azimuthal wave number indicating the rotation around the jet centerline. $A(x)$ is the real amplitude function of x and is to be determined by a nonlinear analysis. For the LEE results, the variables contain both axial and radial information. Only radial information is desired for the integral technique. The radial shape functions are estimated at each axial location by normalizing in the radial direction

$$\int_0^\infty \left(|\hat{u}|^2 + |\hat{v}|^2 + |\hat{w}|^2\right) r\, dr = 1 \quad (9)$$

at each axial location.

Equations of motion

The formulation begins with the following nondimensionalized continuity and momentum equations in cylindrical coordinates:

$$\rho_t + (\rho u)_x + \frac{1}{r}\left[r(\rho v)\right]_r + \frac{1}{r}(\rho w)_\phi = 0 \quad (10)$$

$$\begin{aligned} &(\rho u)_t + \left(\rho u^2 + p\right)_x \\ &\quad + \frac{1}{r}\left[r\left(\rho uv\right)\right]_r + \frac{1}{r}\left(\rho uw\right)_\phi \\ &\quad = \frac{1}{\mathrm{Re}}\boldsymbol{\Delta} u + \frac{1}{3\mathrm{Re}}(\boldsymbol{\nabla}\cdot\boldsymbol{v})_x \end{aligned} \quad (11)$$

$$\begin{aligned} &(\rho v)_t + (\rho uv)_x \\ &\quad + \frac{1}{r}\left[r\left(p + \rho v^2\right)\right]_r + \frac{1}{r}\left(\rho vw\right)_\phi - \frac{\rho w^2}{r} \\ &\quad = \frac{p}{r} + \frac{1}{\mathrm{Re}}\left[\boldsymbol{\Delta} v - \frac{1}{r^2}\left(v + 2w_\phi\right)\right] + \frac{1}{3\mathrm{Re}}(\boldsymbol{\nabla}\cdot\boldsymbol{v})_r \end{aligned} \quad (12)$$

$$\begin{aligned} &(\rho w)_t + (\rho uw)_x \\ &\quad + \frac{1}{r}\left[r\left(\rho vw\right)\right]_r + \frac{1}{r}\left(p + \rho w^2\right)_\phi + \frac{\rho wv}{r} \\ &\quad = \frac{1}{\mathrm{Re}}\left[\boldsymbol{\Delta} w - \frac{1}{r^2}\left(w - 2v_\phi\right)\right] + \frac{1}{3\mathrm{Re}}\frac{1}{r}(\boldsymbol{\nabla}\cdot\boldsymbol{v})_\phi \end{aligned} \quad (13)$$

where the Reynolds number, $\mathrm{Re} = \rho_j U_j D/\mu$, is initially assumed to be constant. The subscripts denote differentiation, the Laplacian is

$$\boldsymbol{\Delta} = \frac{\partial^2}{\partial x^2} + \frac{1}{r}\frac{\partial}{\partial r}r\frac{\partial}{\partial r} + \frac{1}{r^2}\frac{\partial^2}{\partial \phi^2}$$

and

$$\boldsymbol{\nabla}\cdot\boldsymbol{v} = \frac{\partial u}{\partial x} + \frac{1}{r}\frac{\partial}{\partial r}rv + \frac{1}{r}\frac{\partial w}{\partial \phi}.$$

Making substitutions from relations (1) to (6) into (10) to (13), we get:

$$\begin{aligned} &(\overline{\rho} + \rho')_t + \left(\overline{\rho u} + \widetilde{\rho u}\right)_x \\ &\quad + \frac{1}{r}\left[r\left(\overline{\rho v} + \widetilde{\rho v}\right)\right]_r + \frac{1}{r}\left(\overline{\rho w} + \widetilde{\rho w}\right)_\phi = 0 \end{aligned} \quad (14)$$

$$\begin{aligned} &\left(\overline{\rho u} + \widetilde{\rho u}\right)_t + \left[\overline{P} + p' + \left(\overline{U} + u'\right)\left(\overline{\rho u} + \widetilde{\rho u}\right)\right]_x \\ &+ \frac{1}{r}\left[r\left(\overline{V} + v'\right)\left(\overline{\rho u} + \widetilde{\rho u}\right)\right]_r \\ &+ \frac{1}{r}\left[\left(\overline{W} + w'\right)\left(\overline{\rho u} + \widetilde{\rho u}\right)\right]_\phi \\ &= \frac{1}{\mathrm{Re}}\boldsymbol{\Delta}\left(\overline{U} + u'\right) + \frac{1}{3\mathrm{Re}}(\boldsymbol{\nabla}\cdot\overline{\boldsymbol{V}} + \boldsymbol{\nabla}\cdot\boldsymbol{v'})_x \end{aligned} \quad (15)$$

$$\begin{aligned} &\left(\overline{\rho v} + \widetilde{\rho v}\right)_t + \left[\left(\overline{U} + u'\right)\left(\overline{\rho v} + \widetilde{\rho v}\right)\right]_x \\ &+ \frac{1}{r}\left[r\left(\overline{P} + p' + \left(\overline{V} + v'\right)\left(\overline{\rho v} + \widetilde{\rho v}\right)\right)\right]_r \\ &+ \frac{1}{r}\left[\left(\overline{W} + w'\right)\left(\overline{\rho v} + \widetilde{\rho v}\right)\right]_\phi - \frac{1}{r}\left(\overline{W} + w'\right)\left(\overline{\rho w} + \widetilde{\rho w}\right) \\ &= \frac{1}{r}\left(\overline{P} + p'\right) \\ &+ \frac{1}{\mathrm{Re}}\left[\boldsymbol{\Delta}\left(\overline{V} + v'\right) - \frac{1}{r^2}\left(\overline{V} + v' + 2\left(\overline{W} + w'\right)_\phi\right)\right] \\ &+ \frac{1}{3\mathrm{Re}}(\boldsymbol{\nabla}\cdot\overline{\boldsymbol{V}} + \boldsymbol{\nabla}\cdot\boldsymbol{v'})_r \end{aligned} \quad (16)$$

$$\begin{aligned} &\left(\overline{\rho w} + \widetilde{\rho w}\right)_t + \left[\left(\overline{U} + u'\right)\left(\overline{\rho w} + \widetilde{\rho w}\right)\right]_x \\ &+ \frac{1}{r}\left[r\left(\overline{V} + v'\right)\left(\overline{\rho w} + \widetilde{\rho w}\right)\right]_r + \frac{1}{r}\left(\overline{V} + v'\right)\left(\overline{\rho w} + \widetilde{\rho w}\right) \\ &+ \frac{1}{r}\left[\overline{P} + p' + \left(\overline{W} + w'\right)\left(\overline{\rho w} + \widetilde{\rho w}\right)\right]_\phi \\ &= \frac{1}{\mathrm{Re}}\left[\boldsymbol{\Delta}\left(\overline{W} + w'\right) - \frac{1}{r^2}\left(\overline{W} + w' - 2\left(\overline{V} + v'\right)_\phi\right)\right] \\ &+ \frac{1}{3\mathrm{Re}}\frac{1}{r}(\boldsymbol{\nabla}\cdot\overline{\boldsymbol{V}} + \boldsymbol{\nabla}\cdot\boldsymbol{v'})_\phi \end{aligned} \quad (17)$$

These equations will be used to derive a set of equations governing the mean flow and a set of equations governing the large-scale structures.

Mean flow

The mean flow equations are obtained by time-averaging equations (14) to (17) containing the two-component decomposition. The continuity equation for the mean flow is

$$(\overline{\rho u})_x + \frac{1}{r}\left[r\,(\overline{\rho v})\right]_r + \frac{1}{r}\,(\overline{\rho w})_\phi = 0 \tag{18}$$

and the three momentum equations for the mean flow are:

$$\begin{aligned}&\left(\overline{\rho u}\,\overline{U} + \overline{u'\widetilde{\rho u}} + \overline{P}\right)_x + \frac{1}{r}\left[r\left(\overline{\rho u}\,\overline{V} + \overline{v'\widetilde{\rho u}}\right)\right]_r \\ &+ \frac{1}{r}\left(\overline{\rho u}\,\overline{W} + \overline{w'\widetilde{\rho u}}\right)_\phi = \frac{1}{\mathrm{Re}}\boldsymbol{\Delta}\overline{U} + \frac{1}{3\mathrm{Re}}(\boldsymbol{\nabla}\cdot\overline{\boldsymbol{V}})_x\end{aligned} \tag{19}$$

$$\begin{aligned}&\left(\overline{\rho v}\,\overline{U} + \overline{u'\widetilde{\rho v}}\right)_x + \frac{1}{r}\left[r\left(\overline{\rho v}\,\overline{V} + \overline{v'\widetilde{\rho v}} + \overline{P}\right)\right]_r \\ &+ \frac{1}{r}\left(\overline{\rho v}\,\overline{W} + \overline{w'\widetilde{\rho v}}\right)_\phi - \frac{1}{r}\left(\overline{\rho w}\,\overline{W} + \overline{w'\widetilde{\rho w}}\right) \\ &= \frac{1}{r}\overline{P} + \frac{1}{\mathrm{Re}}\left[\boldsymbol{\Delta}\overline{V} - \frac{1}{r^2}\left(\overline{V} + 2\overline{W}_\phi\right)\right] \\ &+ \frac{1}{3\mathrm{Re}}(\boldsymbol{\nabla}\cdot\overline{\boldsymbol{V}})_r\end{aligned} \tag{20}$$

$$\begin{aligned}&\left(\overline{\rho w}\,\overline{U} + \overline{u'\widetilde{\rho w}}\right)_x + \frac{1}{r}\left[r\left(\overline{\rho w}\,\overline{V} + \overline{v'\widetilde{\rho w}}\right)\right]_r \\ &+ \frac{1}{r}\left(\overline{\rho w}\,\overline{W} + \overline{w'\widetilde{\rho w}} + \overline{P}\right)_\phi + \frac{1}{r}\left(\overline{\rho w}\,\overline{V} + \overline{v'\widetilde{\rho w}}\right) \\ &= \frac{1}{\mathrm{Re}}\left[\boldsymbol{\Delta}\overline{W} - \frac{1}{r^2}\left(\overline{W} - 2\overline{V}_\phi\right)\right] + \frac{1}{3\mathrm{Re}}\frac{1}{r}(\boldsymbol{\nabla}\cdot\overline{\boldsymbol{V}})_\phi.\end{aligned} \tag{21}$$

Large-scale structure

The equations governing the large-scale structures are obtained by subtracting the mean flow equations, (18) to (21), from equations (14) to (17). The continuity and momentum equations for the large-scale structures are:

$$\rho'_t + \widetilde{\rho u}_x + \frac{1}{r}\,(r\widetilde{\rho v})_r + \frac{1}{r}\widetilde{\rho w}_\phi = 0 \tag{22}$$

$$\begin{aligned}&\widetilde{\rho u}_t + \left(p' + \overline{\rho u}\,u' + \widetilde{\rho u}\,\overline{U} + \widetilde{\rho u}\,u' - \overline{\widetilde{\rho u}\,u'}\right)_x \\ &+ \frac{1}{r}\left[r\left(\overline{\rho u}\,v' + \widetilde{\rho u}\,\overline{V} + \widetilde{\rho u}\,v' - \overline{\widetilde{\rho u}\,v'}\right)\right]_r \\ &+ \frac{1}{r}\left(\overline{\rho u}\,w' + \widetilde{\rho u}\,\overline{W} + \widetilde{\rho u}\,w' - \overline{\widetilde{\rho u}\,w'}\right)_\phi \\ &= \frac{1}{\mathrm{Re}}\boldsymbol{\Delta}u' + \frac{1}{3\mathrm{Re}}(\boldsymbol{\nabla}\cdot\boldsymbol{v'})_x\end{aligned} \tag{23}$$

$$\begin{aligned}&\widetilde{\rho v}_t + \left(\overline{\rho v}\,u' + \widetilde{\rho v}\,\overline{U} + \widetilde{\rho v}\,u' - \overline{\widetilde{\rho v}\,u'}\right)_x \\ &+ \frac{1}{r}\left[r\left(p' + \overline{\rho v}\,v' + \widetilde{\rho v}\,\overline{V} + \widetilde{\rho v}\,v' - \overline{\widetilde{\rho v}\,v'}\right)\right]_r \\ &+ \frac{1}{r}\left(\overline{\rho v}\,w' + \widetilde{\rho v}\,\overline{W} + \widetilde{\rho v}\,w' - \overline{\widetilde{\rho u}\,w'}\right)_\phi \\ &- \frac{1}{r}\left(\overline{\rho w}\,w' + \widetilde{\rho w}\,\overline{W} + \widetilde{\rho w}\,w' - \overline{\widetilde{\rho w}\,w'}\right) \\ &= \frac{1}{r}p' + \frac{1}{\mathrm{Re}}\left[\boldsymbol{\Delta}v' - \frac{1}{r^2}\left(v' + 2w'_\phi\right)\right] \\ &+ \frac{1}{3\mathrm{Re}}(\boldsymbol{\nabla}\cdot\boldsymbol{v'})_r\end{aligned} \tag{24}$$

$$\begin{aligned}&\widetilde{\rho w}_t + \left(\overline{\rho w}\,u' + \widetilde{\rho w}\,\overline{U} + \widetilde{\rho w}\,u' - \overline{\widetilde{\rho w}\,u'}\right)_x \\ &+ \frac{1}{r}\left[r\left(\overline{\rho w}\,v' + \widetilde{\rho w}\,\overline{V} + \widetilde{\rho w}\,v' - \overline{\widetilde{\rho w}\,v'}\right)\right]_r \\ &+ \frac{1}{r}\left(p' + \overline{\rho w}\,w' + \widetilde{\rho w}\,\overline{W} + \widetilde{\rho w}\,w' - \overline{\widetilde{\rho w}\,w'}\right)_\phi \\ &+ \frac{1}{r}\left(\overline{\rho w}\,v' + \widetilde{\rho w}\,\overline{V} + \widetilde{\rho w}\,v' - \overline{\widetilde{\rho w}\,v'}\right) \\ &= \frac{1}{\mathrm{Re}}\left[\boldsymbol{\Delta}w' - \frac{1}{r^2}\left(w' - 2v'_\phi\right)\right] \\ &+ \frac{1}{3\mathrm{Re}}\frac{1}{r}(\boldsymbol{\nabla}\cdot\boldsymbol{v'})_\phi\end{aligned} \tag{25}$$

Kinetic energy equations

Mean flow kinetic energy equation

The mean flow kinetic energy equation is obtained by first multiplying the x-momentum equation (19) by $\overline{U}$, the r-momentum equation (20) by $\overline{V}$, and the ϕ-momentum equation (21) by $\overline{W}$. Then, the resulting equations are added together. After much manipulation, using the mean flow continuity equation, and defining $K = (\overline{U}^2 + \overline{V}^2 + \overline{W}^2)/2$, the combined equation is rearranged to obtain the kinetic energy equation for the mean flow

$$\begin{aligned}&\frac{\partial}{\partial x}\left(\overline{\rho u}\,K + \overline{\widetilde{\rho u}\,u'}\,\overline{U} + \overline{\widetilde{\rho u}\,v'}\,\overline{V} + \overline{\widetilde{\rho u}\,w'}\,\overline{W}\right) \\ &+ \frac{1}{r}\frac{\partial}{\partial r}\left[r\left(\overline{\rho v}\,K + \overline{\widetilde{\rho v}\,u'}\,\overline{U} + \overline{\widetilde{\rho v}\,v'}\,\overline{V} + \overline{\widetilde{\rho v}\,w'}\,\overline{W}\right)\right] \\ &+ \frac{1}{r}\frac{\partial}{\partial \phi}\left(\overline{\rho w}\,K + \overline{\widetilde{\rho w}\,u'}\,\overline{U} + \overline{\widetilde{\rho w}\,v'}\,\overline{V} + \overline{\widetilde{\rho w}\,w'}\,\overline{W}\right) \\ &+ \overline{U}\,\overline{P}_x + \overline{V}\,\overline{P}_r + \frac{\overline{W}}{r}\overline{P}_\phi \\ &- \overline{U}_x\overline{\widetilde{\rho u}\,u'} - \overline{V}_x\overline{\widetilde{\rho u}\,v'} - \overline{W}_x\overline{\widetilde{\rho u}\,w'} - \overline{U}_r\overline{\widetilde{\rho v}\,u'} \\ &- \overline{V}_r\overline{\widetilde{\rho v}\,v'} - \overline{W}_r\overline{\widetilde{\rho v}\,w'} - \frac{1}{r}\overline{U}_\phi\overline{\widetilde{\rho w}\,u'} - \frac{1}{r}\overline{V}_\phi\overline{\widetilde{\rho w}\,v'} \\ &- \frac{1}{r}\overline{W}_\phi\overline{\widetilde{\rho w}\,w'} - \frac{1}{r}\overline{V}\,\overline{\widetilde{\rho w}\,w'} + \frac{1}{r}\overline{W}\,\overline{\widetilde{\rho w}\,v'} \\ &= \frac{1}{\mathrm{Re}}\Bigg[\boldsymbol{\Delta}K - \left(\overline{U}_{ix}\right)^2 - \left(\overline{U}_{ir}\right)^2 - \frac{1}{r^2}\left(\overline{U}_{i\phi}\right)^2 \\ &\qquad - \frac{\overline{V}}{r^2}\left(\overline{V} + 2\overline{W}_\phi\right) - \frac{\overline{W}}{r^2}\left(\overline{W} - 2\overline{V}_\phi\right)\Bigg] \\ &+ \frac{1}{3\mathrm{Re}}\left[\overline{U}(\boldsymbol{\nabla}\cdot\overline{\boldsymbol{V}})_x + \overline{V}(\boldsymbol{\nabla}\cdot\overline{\boldsymbol{V}})_r + \frac{\overline{W}}{r}(\boldsymbol{\nabla}\cdot\overline{\boldsymbol{V}})_\phi\right]\end{aligned} \tag{26}$$

where $(\overline{U}_{ix})^2 = (\overline{U}_x)^2 + (\overline{V}_x)^2 + (\overline{W}_x)^2$ and similarly for $(\overline{U}_{ir})^2$ and $(\overline{U}_{i\phi})^2$.

Large-scale kinetic energy equation

The large-scale kinetic energy equation is often obtained by multiplying each disturbance momentum equation by its corresponding disturbance velocity and then adding the three equations. This process was used when shape assumptions were based on using locally-parallel, stability calculation results. With LEE, we obtain disturbance variables that are complex. In anticipation of using these complex values, we develop the large-scale kinetic energy equation by multiplying each disturbance momentum equation by the corresponding conjugate disturbance velocity and then adding the conjugate, that is, for the x-momentum equation:

$$u'^*(x\text{-mom.}) + u'(x\text{-mom.})^* \tag{27}$$

Similar equations are derived using the r-momentum equation and the ϕ-momentum equation. After adding these equations together, manipulating extensively, and applying a time-average, the resulting kinetic energy equation for the large-scale structures is

$$\begin{aligned}
&\frac{\partial}{\partial x}(2\overline{\rho u}\,\overline{Q}) + \frac{1}{r}\frac{\partial}{\partial r}(2r\overline{\rho v}\,\overline{Q}) + \frac{1}{r}\frac{\partial}{\partial \phi}(2\overline{\rho w}\,\overline{Q}) \\
&+ \overline{u'^* p'_x} + \overline{v'^* p'_r} + \frac{\overline{w'^* p'_\phi}}{r} \\
&+ \overline{u'^*\widetilde{\rho u}}\,\overline{U}_x + \overline{u'^*\widetilde{\rho v}}\,\overline{U}_r + \frac{\overline{u'^*\widetilde{\rho w}}}{r}\overline{U}_\phi \\
&+ \overline{v'^*\widetilde{\rho u}}\,\overline{V}_x + \overline{v'^*\widetilde{\rho v}}\,\overline{V}_r + \frac{\overline{v'^*\widetilde{\rho w}}}{r}\overline{V}_\phi \\
&+ \overline{w'^*\widetilde{\rho u}}\,\overline{W}_x + \overline{w'^*\widetilde{\rho v}}\,\overline{W}_r + \frac{\overline{w'^*\widetilde{\rho w}}}{r}\overline{W}_\phi \\
&+ \frac{\overline{w'^*\widetilde{\rho w}}}{r}\overline{V} + \frac{\overline{v'^*\widetilde{\rho w}}}{r}\overline{W} + cc + ht \\
&= \frac{1}{\mathrm{Re}}\Bigg[\boldsymbol{\Delta} 2\overline{Q} - \overline{u'^*_{ix}u'_{ix}} - \overline{u'^*_{ir}u'_{ir}} - \frac{\overline{u'^*_{i\phi}u'_{i\phi}}}{r^2} \\
&\qquad - \frac{\overline{v'^*}}{r^2}(v' + 2w'_\phi) - \overline{\frac{w'^*}{r^2}(w' - 2v'_\phi)} + cc\Bigg] \\
&+ \frac{1}{3\mathrm{Re}}\Bigg[\overline{u'^*(\boldsymbol{\nabla}\cdot\boldsymbol{v'})_x} + \overline{v'^*(\boldsymbol{\nabla}\cdot\boldsymbol{v'})_r} \\
&\qquad + \overline{\frac{w'^*}{r}(\boldsymbol{\nabla}\cdot\boldsymbol{v'})_\phi} + cc\Bigg]
\end{aligned} \tag{28}$$

where $Q = (|u'|^2 + |v'|^2 + |w'|^2)/2$, cc denotes the complex conjugate of the preceding complex terms, and ht denotes higher order terms containing the product of three or more disturbance variables.

When the shape assumption given by equation (8) is applied in equation (28), the axial derivatives will decompose into two terms; one for the derivative of the amplitude function $A(x)$ and one for the derivative of the phase function $\psi(x)$. Thus, an additional equation is required to describe the axial evolution of the phase. Following Lee & Liu,[12] this is obtained by first subtracting the momentum equations, rather than adding as in equation (27),

$$u'^*(x\text{-mom.}) - u'(x\text{-mom.})^* \tag{29}$$

This equation and the additional two equations for the r- and ϕ-momentum equations are added together and extensively manipulated. The resulting equation is more complicated than equation (28) and will not be given. Only the final integrated equation will be given below.

INTEGRAL FORM OF THE ENERGY EQUATION

For the round jet, the mean quantities are assumed to be axisymmetric. Thus, $\overline{W} = 0$ and $\partial(\overline{\ \ })/\partial\phi = 0$. The energy equations (26) and (28) for the mean flow and the large-scale structures, respectively, are simplified as these terms are removed. Then, the usual boundary-layer-type approximations are applied to the mean quantities. The mean radial velocity is much less than the mean axial velocity, $\overline{V} \ll \overline{U}$, and the axial gradients are much less than the radial gradients, $\partial(\overline{\ \ })/\partial x \ll \partial(\overline{\ \ })/\partial r$. Using these approximations and considering the number of disturbance variables in each term, the terms are ordered in size and those terms up to second order are retained. The mean flow pressure is then assumed to be constant across the jet. Finally, multiplying by r and integrating over r, the integral form of the mean energy equation reduces to the following simple form.

$$\begin{aligned}
&\frac{d}{dx}\int_0^\infty \left(\frac{1}{2}\overline{\rho u}\,\overline{U}^2 + \overline{\widetilde{\rho u}u'}\,\overline{U}\right) r dr \\
&= \int_0^\infty \overline{\widetilde{\rho u}u'}\,\overline{U}_x r dr + \int_0^\infty \overline{\widetilde{\rho v}u'}\,\overline{U}_r r dr \\
&+ \int_0^\infty \overline{\rho}\,\overline{v'v'}\,\overline{V}_r r dr + \int_0^\infty \overline{\rho}\,\overline{V}\,\overline{w'w'} dr \\
&- \frac{1}{\mathrm{Re}}\int_0^\infty (\overline{U}_r)^2 r dr
\end{aligned} \tag{30}$$

Similarly, the energy equation for the large-scale structure component reduces to:

$$\begin{aligned}
&\frac{d}{dx}\int_0^\infty (2\overline{\rho}\,\overline{U}\,\overline{Q}) r dr = \\
&- \int_0^\infty \left(\overline{u'^* p'_x} + \overline{v'^* p'_r} + \frac{\overline{w'^* p'_\phi}}{r} + cc\right) r dr \\
&- \int_0^\infty \left(\overline{u'^*\widetilde{\rho u}}\,\overline{U}_x + \overline{u'^*\widetilde{\rho v}}\,\overline{U}_r + cc\right) r dr \\
&- \int_0^\infty \left(\overline{\rho}\,\overline{v'^* v'}\,\overline{V}_r + \frac{\overline{\rho}\,\overline{w'^* w'}}{r}\overline{V} + cc\right) r dr
\end{aligned}$$

$$- \frac{1}{\mathrm{Re}} \int_0^\infty \left[\overline{u_{ix}'^* u_{ix}'} + \overline{u_{ir}'^* u_{ir}'} + \frac{\overline{u_{i\phi}'^* u_{i\phi}'}}{r^2} \right. \tag{31}$$
$$\left. + \overline{\frac{v'^*}{r^2}(v' + 2w_\phi')} + \overline{\frac{w'^*}{r^2}(w' - 2v_\phi')} + cc \right] r dr$$
$$+ \frac{1}{3\mathrm{Re}} \int_0^\infty \left[\overline{u'^* (\boldsymbol{\nabla} \cdot \boldsymbol{v'})_x} + \overline{v'^* (\boldsymbol{\nabla} \cdot \boldsymbol{v'})_r} \right.$$
$$\left. + \overline{\frac{w'^*}{r} (\boldsymbol{\nabla} \cdot \boldsymbol{v'})_\phi} + cc \right] r dr$$

In this equation, terms to second order are retained and those terms involving the second derivative with respect to x are neglected. For terms higher than second order, the time-average is zero when using the shape assumption, equation (8).

The physical interpretation of the terms appearing in the energy equations is obvious. For the mean flow equation, the first term on the left side is the mean flow advection of the mean flow kinetic energy, the second term involves energy transfer. The first four terms on the right-hand side of (30) govern the energy transfer from the mean flow to the coherent structure, and the last term is the viscous dissipation of the mean flow energy. As for the large-scale equation (31); the left-hand side is the mean flow advection of the large-scale kinetic energy. The first term on the right-hand side is the work done by the large-scale pressure gradients, the next two terms are the energy transfer from the mean flow to the large-scale structures, and the last two terms are the large-scale energy dissipation.

When substituting the mode definitions into equation (30) for the mean energy, we will assume that the disturbances are real. Hence, each disturbance variable is represented by equation (8) plus its complex conjugate. The time-averaging process results in the following ordinary differential equation.

$$\frac{d\theta}{dx}\frac{dI_{am}}{d\theta} + \frac{d}{dx}\left[A^2 I_{at}\right] = A^2 I_{mwt} - \frac{1}{\mathrm{Re}} I_{md} \tag{32}$$

In this analysis, the mean flow is characterized by the momentum thickness rather than by the axial distance. Hence, the integrals in the energy equations are dependent on θ instead of x.

For both the large-scale energy equation (31) and the phase equation, the disturbance variables are used in their complex form as given in equation (8). The resulting ordinary differential equations are:

$$\frac{d}{dx}\left[A^2 I_{aw}\right] + \frac{dA^2}{dx} I_{p1b} - A^2 \frac{d\psi}{dx} 2 I_{wp1a} \tag{33}$$
$$= A^2 \left(-I_{mwt} - I_{pt} - \frac{1}{\mathrm{Re}} I_{wd} - \frac{1}{3\mathrm{Re}} I_{wc} \right)$$

and

$$\frac{1}{2}\frac{dA^2}{dx} I_{wp1b} + A^2 \frac{d\psi}{dx}\left[I_{aw} + I_{p1}\right] \tag{34}$$
$$= A^2 \left(\omega I_f + I_{pht} - I_{wpt}\right)$$

All the integral terms in equations (32) to (34) are given in the Appendix. Note that unlike in the previous paper,[4] all the energy transfer integrals appearing in equation (32), represented by I_{mwt}, appear identically in equation (33) with opposite sign, as expected.

NUMERICAL RESULTS

The calculations were performed for three, perfectly expanded jets with exit Mach numbers of 1.5, 1.8, and 2.1. In all cases, the jets were cold with the jet exit total temperature equal to the ambient temperature. The mean flow was computed using the parabolized, boundary-layer procedure of Dahl & Morris[13] with the addition that the radial velocity profile was computed from the mean continuity equation. This procedure generated mean flow profiles that smoothly transition from the initial region to the fully developed region allowing complete parameterization by the momentum thickness, θ, as required by the nonlinear analysis.

The mean flow was used in the Linearized Euler Equation (LEE) solver described in a previous section. The time-domain solver was run until initial transients ended. The unsteady disturbance flow field was then stored at constant time intervals creating time histories of all the computed unsteady flow variables at each grid point of the flow field. The time interval corresponds to $1/8$th of the period for the frequency used for the inflow disturbance. In our calculations here, the frequency corresponds to a Strouhal number $fD/U_j = 0.2$ and $n = 1$ for the azimuthal mode number. An example of the computed pressure disturbance field is shown in Figure 1. The pressure disturbance contours exhibit a growth and decay behavior within the jet and a radiation directivity characteristic outside of the jet. The pressure disturbance also decays with distance away from the jet. These results are typical for all three computed jets.

The set of disturbance flow fields from the LEE calculations were post-processed to provide the data for the nonlinear integral calculations. After taking the Fourier Transform in time to obtain the complex amplitude of each unsteady flow variable at each grid point, the data were normalized according to equation (9) to obtain the radial shape functions for each variable. The radial shape functions are then used to compute the integrals that appear in equations (32) to (34), the set of coupled ordinary differential equations for the mean flow momentum thickness θ, the disturbance variable amplitude A^2, and the disturbance variable axial phase function ψ. Since the integrals are considered to be functions of θ, interpolations were made of

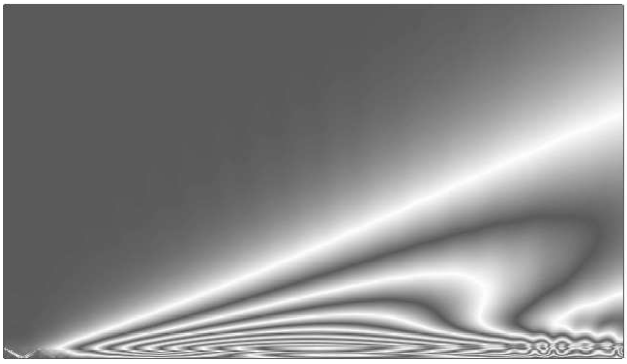

Fig. 1 LEE computed pressure disturbance field. $\mathbf{M_j = 2.1}$; $\mathbf{fD/U_j = 0.2}$; $\mathbf{n = 1}$.

these integral functions during the solution of the differential equations. The differential equations were manipulated to form three first-order, coupled, initial-value differential equations that were solved by implementing a degree-1 Taylor series scheme with fixed point iteration.[14] Only the choice of the initial amplitude was needed to start the integration at $x = 0$. The initial value for θ was given by the mean flow calculations and the initial value for the phase function ψ was set to zero. Any nonzero initial value for ψ merely offset all the results for ψ by that initial nonzero value.

Effect of Re

The differential equations contain a Reynolds number that comes from the normalized Navier-Stokes equations. Obviously the Euler equations are inviscid, hence the Reynolds number must be provided by the underlying mean flow. Solutions for the amplitude function are shown for the $M_j = 1.8$ jet in Figure 2 for two different initial amplitudes, $A_o^2 = 10^{-7}$ and $A_o^2 = 10^{-3}$. Given that we consider the jets to be high-Reynolds number turbulent jets, the high constant Reynolds number results show growth but very little decay for the amplitude. If we consider the viscosity to be a turbulent viscosity, as in Tam & Chen,[15] and choose a smaller constant Reynolds number, we see that significant 'early' decay does not begin until the Reynolds number is getting relatively small. To avoid the arbitrary choice of a Reynolds number, we follow our previous procedure by choosing a local variable Reynolds number obtained from the mean flow calculations.[4] This is a simple way to mimic the increased effects of fine-scale turbulence on dissipating the energy in the large-scale turbulence as the large structure moves downstream. The amplitude results using the variable Re approach is also shown in Figure 2.

Local energy integrals

The four integral terms in equation (32) govern the advection, transfer, and dissipation of the mean kinetic energy. Using the data computed by the LEE code, these

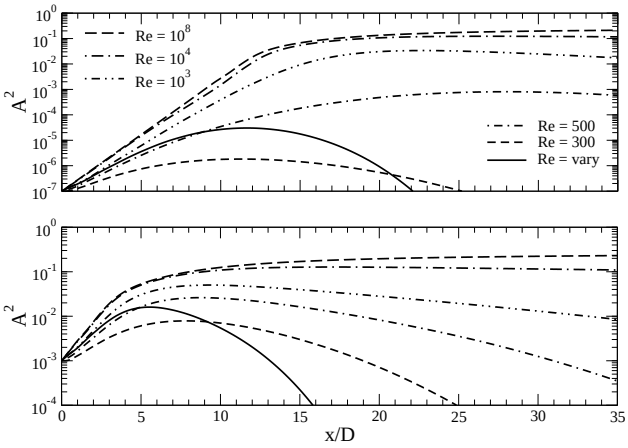

Fig. 2 Amplitude function comparisons showing effects of Reynolds number. $\mathbf{M_j = 1.8}$; $\mathbf{fD/U_j = 0.2}$; $\mathbf{n = 1}$.

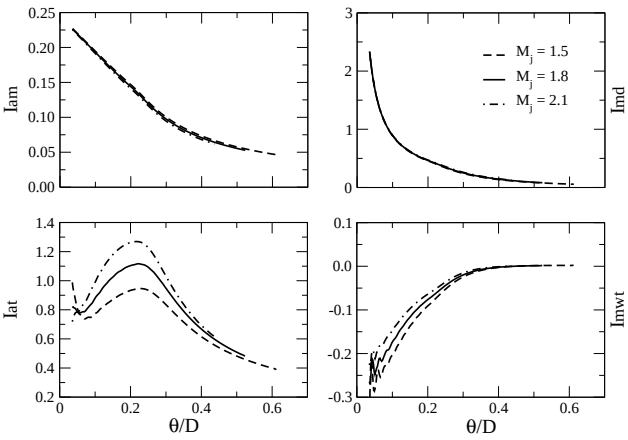

Fig. 3 Energy integrals from the mean flow energy equation (32). $\mathbf{fD/U_j = 0.2}$; $\mathbf{n = 1}$.

integrals are computed using the trapezoidal rule and the results are plotted in Figure 3 for the three jet Mach numbers. Due to the transient waves present near the inflow boundary, the integral calculations were started at $\theta/D = 0.035$. As functions of θ, the two integrals that depend solely on the mean flow, I_{am} and I_{md}, are nearly identical for the three jets. The integral I_{am} represents the advection of the mean flow kinetic energy. The rate of change of I_{am} is initially constant and then gradually decreases. The energy moves downstream as the jet spreads and then the advection slows downstream of the potential core. The I_{md} integral represents viscous dissipation of the mean kinetic energy. It starts out initially high due to the high radial gradients of the axial mean velocity. It steadily decreases in value as the flow proceeds downstream.

The I_{mwt} integral governs the main transfer of energy from the mean flow to the large-scale structures. It is entirely negative as the jet evolves, indicating that energy is only transferred from the mean flow to the large-scale structures and not the reverse. Its magnitude is largest

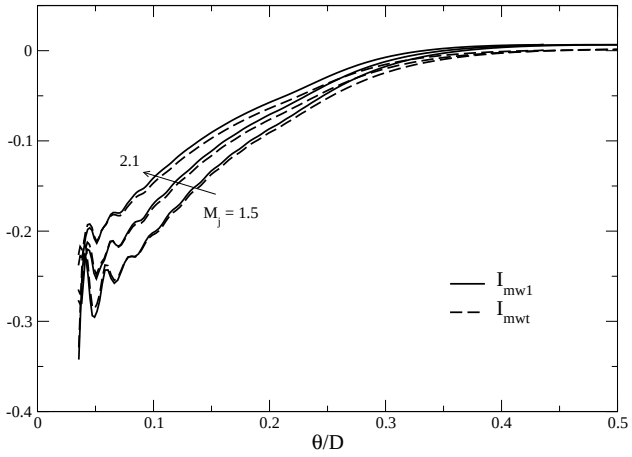

Fig. 4 Comparison of energy transfer integrals. $\mathbf{I_{mw1}}$ is dominant integral. $\mathbf{I_{mwt}}$ is $\mathbf{I_{mw1}}$ plus second order integrals.

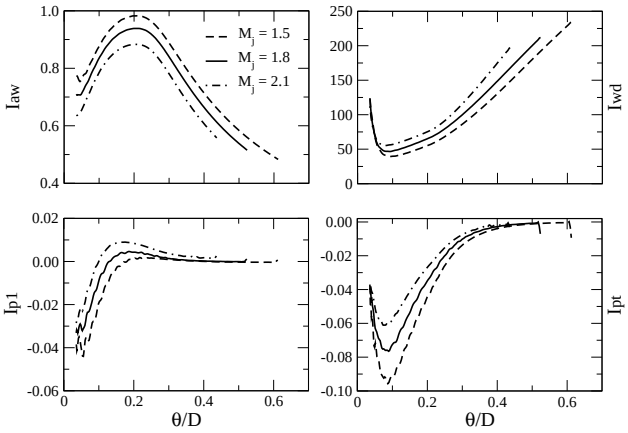

Fig. 5 Energy integrals from the large-scale structure energy equation (33). $\mathbf{fD/U_j = 0.2;\ n = 1.}$

for the lowest Mach number and it decreases as the Mach number increases becoming a less efficient energy transfer process. In the current derivation, I_{mwt} consists of the sum of six terms, the largest, I_{mw1}, has the classical form for the velocity-shear driven generation of the large-scale structures (See Appendix). To various degrees, the additional terms add effects of compressibility and non-parallel flow to the energy transfer process. As can be seen in Figure 4, these additional integrals add little to the total energy transfer integral in these cold, slowly diverging jets. The waviness seen in the initial part of the plots of I_{mwt} in Figure 3 are remnants of the problems with the inflow boundary condition.

The only way to possibly transfer energy from the large-scale structures back to the mean flow is via the I_{at} integral. The general behavior of I_{at} is to increase to a maximum value and then decrease downstream. The initial positive gradient is indicative of energy transfer towards the large-scale structures. After the peak and the gradient becomes negative, then some energy can be transferred from the large-scale structures to the mean flow. Both the magnitude and the gradients each side of the peak increase as the Mach number increased.

Figure 5 shows four of the dominant integral terms in equation (33) governing the kinetic energy in the large-scale structures. The integral for the advection of the large-scale kinetic energy, I_{aw}, increases as the energy flows in from the mean flow. Once dissipating mechanisms take over, the integral decreases in value. The lower values of I_{aw} as Mach number increases corresponds to the lower levels of incoming energy from the higher mean flows. The large-scale energy decreases as I_{wd}, the dissipation integral, increases. The remaining two integrals shown represent work done by the large-scale structure pressure gradients; I_{p1} represents work done by the axial pressure gradients and I_{pt} represents work done by both the radial and the azimuthal pressure gradients. Both integrals are relatively small in magnitude. These integrals are the only ones using the pressure disturbance and their behavior at the computed flow field exit indicates the presence of reflections from the outflow boundary.

Nonlinear amplitude

The results for the computed amplitude function for the jet with Mach number 1.8 are shown in Figure 6. The initial amplitude A_o^2 varies from 10^{-7} to 10^{-1}. Part (a) shows the absolute value of the amplitude and part (b) shows the amplitude normalized by the initial amplitude. Notice that when the amplitude is normalized, the $A_o^2 = 10^{-7}$ and 10^{-6} plots are basically identical. This indicates a linear response. The amplitude function changed by the same amount as the change in the initial amplitude. The normalized plot for $A_o^2 = 10^{-5}$ begins to deviate from the previous normalized plots at about $x/D = 10$. In part (a), it is seen that the $A_o^2 = 10^{-5}$ plot is exceeding approximately 10^{-3} at that location. This pattern holds for higher initial amplitudes indicating an amplitude threshold above which nonlinear effects take place. At the initial amplitude of 10^{-1}, growth has nearly ceased and single frequency saturation starts to occur.[16]

Using initial amplitudes of 10^{-2} and 10^{-7} to generate nonlinear and linear responses, respectively, for the amplitude function, Figure 7 shows comparisons for the three jet Mach numbers. The amplitude of the linear response grows in amplitude as the Mach number increases. As the initial amplitude increases and nonlinear effects become more important, the Mach number has very little effect on the maximum large-scale structure amplitude.

The energy integral equations also compute the change in mean flow momentum thickness and large-scale structure phase function. Results are shown in Figure 8. Part (a) shows that the momentum thickness remains unchanged for small initial amplitudes. It is through the nonlinear process that the momentum thickness increases at the higher amplitudes until saturation. In part (b), the momentum thick-

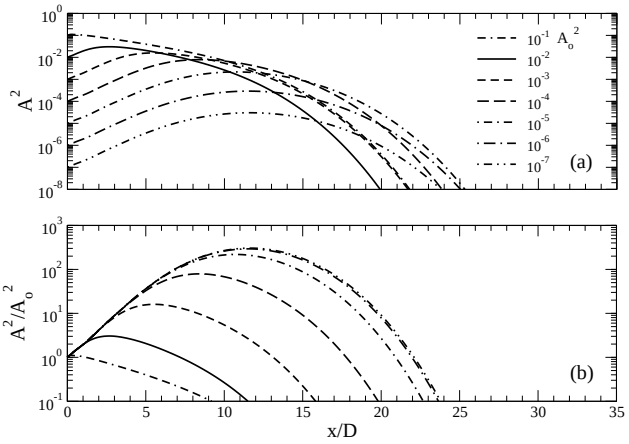

Fig. 6 Amplitude function comparisons with different initial amplitudes. (a) Absolute amplitude. (b) Amplitude normalized by initial amplitude. $M_j = 1.8$; $fD/U_j = 0.2$; $n = 1$.

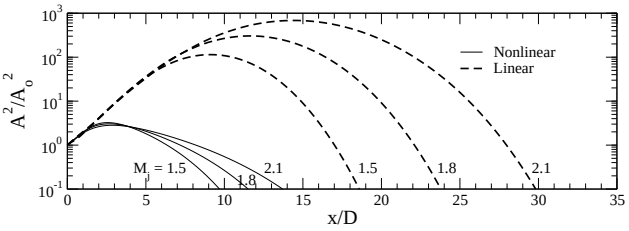

Fig. 7 Amplitude function comparisons between nonlinear and linear calculations at different Mach numbers. Nonlinear: $A_o^2 = 10^{-2}$. Linear: $A_o^2 = 10^{-7}$. $fD/U_j = 0.2$; $n = 1$.

ness decreases downstream as the Mach number increases where initially the behavior of the momentum thickness is similar for all three jets. Finally, the phase function is plotted in part (c) as a phase speed for the large-scale structure. Nonlinearity has the effect of a rapid increase in phase speed near the nozzle exit compared to the gradual change in phase speed seen in the linear case.

CONCLUDING REMARKS

The Linearized Euler Equation method, with given nonparallel mean flow, has been used to compute the large-scale turbulent structures. Normalized radial functions were derived from this data to be used in the energy integral method that describes the weakly nonlinear interactions of a growing large-scale structure with the mean flow. Below some initial amplitude threshold, the evolving disturbances behave linearly. Above that threshold, the amplitude of the disturbance peaks and decays earlier in axial location compared to the linear response. These results were also shown to be highly dependent on the dissipation model used for the large-scale structures.

REFERENCES

1. M. E. Goldstein. A unified approach to some recent developments in jet noise theory. *Int. J. of Aeroacoustics*, 1:1–16, 2002.

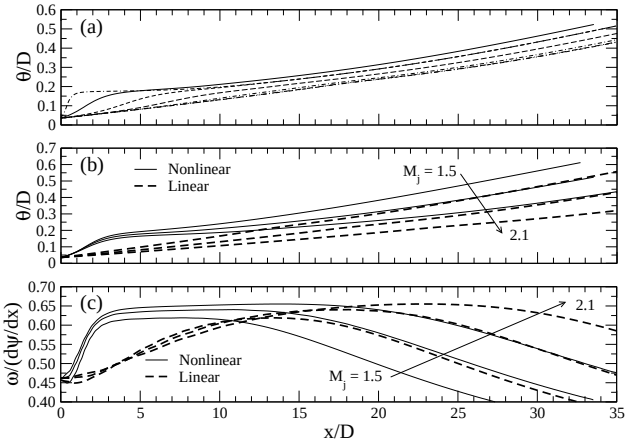

Fig. 8 Comparisons of shear layer growth and large-scale phase velocity. (a) Momentum thickness; legend in Fig. 6. (b) Momentum thickness for 3 jets of Fig. 7. (c) Large-scale phase velocity for 3 jets of Fig. 7.

2. A. Khavaran. Role of anisotropy in turbulence mixing noise. *AIAA J.*, 37(7):832–841, 1999.

3. C. K. W. Tam and L. Auriault. Jet mixing noise from fine-scale turbulence. *AIAA J.*, 37(2):145–153, 1999.

4. M. D. Dahl and R. R. Mankbadi. Analysis of three-dimensional, nonlinear development of wave-like structure in a compressible round jet. AIAA Paper No. 2002-2451, 2002.

5. V. V. Golubev, A. Prieto, L. Bueno, R. R. Mankbadi, and M. D. Dahl. Comparison of several approaches to predict noise associated with jet acoustic source models. AIAA Paper No. 2003-3283, 2003.

6. D. Stanescu and W. G. Habashi. 2N-storage low dissipation and dispersion Runge-Kutta schemes for computational acoustics. *J. Comp. Phys.*, 143:674–681, 1998.

7. F. Q. Hu, M. Y. Hussaini, and J. L. Manthey. Low-dissipation and low-dispersion Runge-Kutta schemes for computational acoustics. *J. Comp. Phys.*, 124:177–191, 1996.

8. C. K. W. Tam and J. C. Webb. Dispersion-relation-preserving finite difference schemes for computational acoustics. *J. Comp. Phys.*, 107:262–281, 1993.

9. C. A. Kennedy and M. H. Carpenter. Several new numerical methods for compressible shear-layer simulations. *Appl. Num. Math.*, 14:397–433, 1994.

10. R. R. Mankbadi, R. Hixon, S. H. Shih, and L. A. Povinelli. Use of linearized Euler equations for supersonic jet noise prediction. *AIAA J.*, 36:140–147, 1998.

11. S. H. Shih, D. R. Hixon, and R. R. Mankbadi. Three dimensional large eddy simulation: Behavior near centerline. *Int. J. of Comp. Fluid Dyn.*, 2:109–123, 2000.

12. S. S. Lee and J. T. C. Liu. Multiple coherent mode interactions in a developing round jet. *J. Fluid Mech.*, 248:383–401, 1993.

13. M. D. Dahl and P. J. Morris. Noise from supersonic coaxial jets, part 1: Mean flow predictions. *J. Sound Vib.*, 200:643–663, 1997.

14. J. R. Scott. Solving ODE initial value problems with implicit Taylor series methods. NASA TM-2000-209400, 2000.

15. C. K. W. Tam and K. C. Chen. A statistical model of turbulence in two-dimensional mixing layers. *J. Fluid Mech.*, 92:303–326, 1979.

16. R. R. Mankbadi and J. T. C. Liu. A study of the interactions between large-scale coherent structures and fine-grained turbulence in a round jet. *Phil. Trans. R. Soc. Lond. A*, 298:541–602, 1981.

APPENDIX

$\Re$ = Real Part $\quad \Im$ = Imaginary Part

$$I_{am} = \frac{1}{2}\int_0^\infty \overline{\rho}\,\overline{U}^3 r\,dr \qquad I_{md} = \int_0^\infty \left(\frac{\partial \overline{U}}{\partial r}\right)^2 r\,dr$$

$$I_{at} = \int_0^\infty \left[3\Re\{\hat{u}^*\hat{\rho}\}\overline{U}^2 + 2|\hat{u}|^2\overline{\rho}\,\overline{U}\right] r\,dr$$

$$I_{mwt} = I_{mw1} + I_{mw3} + I_{mw4} + I_{mw5} + I_{mw6} + I_{mw7}$$

$$I_{mw1} = 2\int_0^\infty \Re\{\hat{v}^*\hat{u}\}\overline{\rho}\,\frac{\partial \overline{U}}{\partial r} r\,dr$$

$$I_{mw3} = 2\int_0^\infty \Re\{\hat{u}^*\hat{\rho}\}\overline{V}\,\frac{\partial \overline{U}}{\partial r} r\,dr$$

$$I_{mw4} = 2\int_0^\infty \Re\{\hat{u}^*\hat{\rho}\}\overline{U}\,\frac{\partial \overline{U}}{\partial x} r\,dr$$

$$I_{mw5} = 2\int_0^\infty |\hat{u}|^2\overline{\rho}\,\frac{\partial \overline{U}}{\partial x} r\,dr$$

$$I_{mw6} = 2\int_0^\infty |\hat{v}|^2\overline{\rho}\,\frac{\partial \overline{V}}{\partial r} r\,dr \quad I_{mw7} = 2\int_0^\infty |\hat{w}|^2\overline{\rho}\,\overline{V}\,dr$$

$$I_{aw} = \int_0^\infty \left(|\hat{u}|^2 + |\hat{v}|^2 + |\hat{w}|^2\right)\overline{\rho}\,\overline{U} r\,dr$$

$$I_{p1b} = I_{p1} + \frac{1}{3\mathrm{Re}} I_{wca} \qquad I_{wp1a} = I_{wp1} - \frac{1}{6\mathrm{Re}} I_{wcp}$$

$$I_{p1} = \int_0^\infty \Re\{\hat{u}^*\hat{p}\} r\,dr \qquad I_{wp1} = \int_0^\infty \Im\{\hat{u}^*\hat{p}\} r\,dr$$

$$I_{wca} = \int_0^\infty \left[\left(\Re\left\{\hat{v}^*\frac{\partial \hat{u}}{\partial r}\right\} + \Re\left\{\hat{u}^*\frac{\partial \hat{v}}{\partial r}\right\}\right) r + \Re\{\hat{v}^*\hat{u}\}\right] dr$$

$$I_{wcp} = \int_0^\infty \left[2\left(\Im\left\{\hat{v}^*\frac{\partial \hat{u}}{\partial r}\right\} + \Im\left\{\hat{u}^*\frac{\partial \hat{v}}{\partial r}\right\}\right) r - \Im\{\hat{v}^*\hat{u}\} + 2n\Re\{\hat{u}^*\hat{w}\}\right] dr$$

$$I_{pt} = 2\int_0^\infty \left[\Re\left\{\hat{v}^*\frac{\partial \hat{p}}{\partial r}\right\} - n\Im\{\hat{w}^*\hat{p}\}\right] dr$$

$$I_{wd} = 2\int_0^\infty \left[\frac{n^2}{r^2}\left(|\hat{u}|^2 + |\hat{v}|^2 + |\hat{w}|^2\right) + \frac{1}{r^2}\left(|\hat{v}|^2 + |\hat{w}|^2\right) - \frac{4n}{r^2}\Im\{\hat{v}^*\hat{w}\} + \left(\left|\frac{\partial \hat{u}}{\partial r}\right|^2 + \left|\frac{\partial \hat{v}}{\partial r}\right|^2 + \left|\frac{\partial \hat{w}}{\partial r}\right|^2\right)\right] r\,dr$$

$$I_{wc} = 2\int_0^\infty \left[\left(\left|\frac{\partial \hat{v}}{\partial r}\right|^2 + \frac{n^2}{r^2}|\hat{w}|^2 + \frac{1}{r^2}|\hat{v}|^2 - \frac{2n}{r^2}\Im\{\hat{v}^*\hat{w}\}\right) r + n\left(\Im\left\{\hat{v}^*\frac{\partial \hat{w}}{\partial r}\right\} + \Im\left\{\hat{w}^*\frac{\partial \hat{v}}{\partial r}\right\}\right)\right] dr$$

$$I_{wp1b} = I_{wp1} - \frac{2}{3\mathrm{Re}} I_{mp}$$

$$I_{mp} = \int_0^\infty \left[\Im\left\{\hat{v}^*\frac{\partial \hat{u}}{\partial r}\right\} r + n\Re\{\hat{u}^*\hat{w}\}\right] dr$$

$$I_f = \int_0^\infty \left(|\hat{u}|^2 + |\hat{v}|^2 + |\hat{w}|^2\right)\overline{\rho}\, r\,dr$$

$$I_{wpt} = \int_0^\infty \left[\Im\left\{\hat{v}^*\frac{\partial \hat{p}}{\partial r}\right\} r + n\Re\{\hat{w}^*\hat{p}\}\right] dr$$

$$I_{pht} = I_{ph1} - I_{ph2} - I_{ph3} - I_{ph4} - I_{ph5} - I_{ph6} - I_{ph7}$$

$$I_{ph1} = \int_0^\infty \Im\{\hat{v}^*\hat{u}\}\overline{\rho}\,\frac{\partial \overline{U}}{\partial r} r\,dr$$

$$I_{ph2} = \int_0^\infty \left[\Im\left\{\hat{u}^*\frac{\partial \hat{u}}{\partial r}\right\} + \Im\left\{\hat{v}^*\frac{\partial \hat{v}}{\partial r}\right\} + \Im\left\{\hat{w}^*\frac{\partial \hat{w}}{\partial r}\right\}\right]\overline{\rho}\,\overline{V} r\,dr$$

$$I_{ph3} = \int_0^\infty \Im\{\hat{u}^*\hat{\rho}\}\overline{V}\,\frac{\partial \overline{U}}{\partial r} r\,dr$$

$$I_{ph4} = \int_0^\infty \Im\{\hat{u}^*\hat{\rho}\}\overline{U}\,\frac{\partial \overline{U}}{\partial x} r\,dr$$

$$I_{ph5} = \int_0^\infty \Im\{\hat{v}^*\hat{\rho}\}\overline{U}\,\frac{\partial \overline{V}}{\partial x} r\,dr$$

$$I_{ph6} = \int_0^\infty \Im\{\hat{v}^*\hat{u}\}\overline{\rho}\,\frac{\partial \overline{V}}{\partial x} r\,dr$$

$$I_{ph7} = \int_0^\infty \Im\{\hat{v}^*\hat{\rho}\}\overline{V}\,\frac{\partial \overline{V}}{\partial r} r\,dr$$

REPORT DOCUMENTATION PAGE

Form Approved
OMB No. 0704-0188

1. AGENCY USE ONLY (*Leave blank*)	2. REPORT DATE	3. REPORT TYPE AND DATES COVERED
	July 2003	Technical Memorandum

4. TITLE AND SUBTITLE

Computation of Large-Scale Structure Jet Noise Sources With Weak Nonlinear Effects Using Linear Euler

5. FUNDING NUMBERS

WBS–22–781–30–12

6. AUTHOR(S)

Milo D. Dahl, Ray Hixon, and Reda R. Mankbadi

7. PERFORMING ORGANIZATION NAME(S) AND ADDRESS(ES)

National Aeronautics and Space Administration
John H. Glenn Research Center at Lewis Field
Cleveland, Ohio 44135–3191

8. PERFORMING ORGANIZATION REPORT NUMBER

E–13960

9. SPONSORING/MONITORING AGENCY NAME(S) AND ADDRESS(ES)

National Aeronautics and Space Administration
Washington, DC 20546–0001

10. SPONSORING/MONITORING AGENCY REPORT NUMBER

NASA TM—2003-212383
AIAA–2003–3254

11. SUPPLEMENTARY NOTES

Prepared for the Nineth Aeroacoustics Conference and Exhibit cosponsored by the American Institute of Aeronautics and Astronautics and the Confederation of European Aerospace Societies, Hilton Head, South Carolina, May 12–14, 2003. Milo D. Dahl, NASA Glenn Research Center; Ray Hixon, University of Toledo, Toledo, Ohio 43606; Reda R. Mankbadi, Embry-Riddle Aeronautical University, Daytona Beach, Florida 32114. Responsible person, Milo D. Dahl, organization code 5940, 216–433–3578.

12a. DISTRIBUTION/AVAILABILITY STATEMENT

Unclassified - Unlimited
Subject Category: 71 Distribution: Nonstandard

Available electronically at http://gltrs.grc.nasa.gov

This publication is available from the NASA Center for AeroSpace Information, 301–621–0390.

12b. DISTRIBUTION CODE

13. ABSTRACT ***(Maximum 200 words)***

An approximate technique is presented for the prediction of the large-scale turbulent structure sound source in a supersonic jet. A linearized Euler equations code is used to solve for the flow disturbances within and near a jet with a given mean flow. Assuming a normal mode composition for the wave-like disturbances, the linear radial profiles are used in an integration of the Navier-Stokes equations. This results in a set of ordinary differential equations representing the weakly nonlinear self-interactions of the modes along with their interaction with the mean flow. Solutions are then used to correct the amplitude of the disturbances that represent the source of large-scale turbulent structure sound in the jet.

14. SUBJECT TERMS

Jet noise; Jet source prediction; Nonlinear instability; Computational aeroacoustics

15. NUMBER OF PAGES
18

16. PRICE CODE

17. SECURITY CLASSIFICATION OF REPORT	18. SECURITY CLASSIFICATION OF THIS PAGE	19. SECURITY CLASSIFICATION OF ABSTRACT	20. LIMITATION OF ABSTRACT
Unclassified	Unclassified	Unclassified	